Materials Science & Engineering A 581 (2013) 140–144

Contents lists available at SciVerse ScienceDirect

Materials Science & Engineering A

journal homepage: www.elsevier.com/locate/msea

Fracture characteristics of freestanding 8 wt% Y_2O_3–ZrO_2 coatings by single edge notched beam and Vickers indentation tests

J. Wan [a,b], M. Zhou [a,b], X.S. Yang [a,b], C.Y. Dai [a,b], Y. Zhang [a,b], W.G. Mao [a,b,*], C. Lu [c]

[a] Key Laboratory of Low Dimensional Materials & Application Technology, Ministry of Education, Xiangtan University, Hunan 411105, China
[b] Faculty of Materials, Optoelectronics and Physics, Xiangtan University, Hunan 411105, China
[c] Department of Mechanical Engineering, Curtin University, Western Australia 6845, Australia

ARTICLE INFO

Article history:
Received 26 February 2013
Received in revised form
14 May 2013
Accepted 17 May 2013
Available online 14 June 2013

Keywords:
Thermal barrier coating
Fracture toughness
Single edge notched beam
Vickers indentation
Digital image correlation

ABSTRACT

The freestanding 8 wt% Y_2O_3–ZrO_2 (8YSZ) samples prepared by an air plasma sprayed technique were measured by single edge notched bending tests. The strain evolution and cracking near a pre-existed notch region were *in-situ* monitored by digital image correlation. With the help of digital image data, the critical bending loads of these notched freestanding 8YSZ samples can be accurately determined. The fracture toughness and micro-hardness of freestanding 8YSZ samples were tested by Vickers indentations. The normalized fracture toughness calculated according to the Weibull statistics is in agreement with the testing and available data. These results are instructive in predicting the lifetime and durability of thermal barrier coatings with irregular geometric structures.

1. Introduction

Thermal barrier coatings (TBCs) have attracted an increasing attention in aircraft and industrial gas-turbine applications because of their excellent wear resistance, corrosion proof, and thermal insulation [1,2]. The merits of using ceramic TBCs are well recognized in the increase of engine operating temperature with reduced cooling requirements, resulting in significant improvements of thermal efficiency, performance and reliability [3]. The 8 wt% yttria stabilized zirconia (8YSZ) ceramics have been commonly regarded as a crucial thermal insulation material. However, the phase transformation, high-temperature sintering and oxidation, mismatch between thermal and residual stresses, and creep of YSZ coatings are inevitable in practice, which may accelerate the spallation and failure of TBCs [2–6]. Therefore, the evolution of mechanical, physical and chemical properties of 8YSZ coatings during thermal cycling plays an important role in predicting their durability and reliability. In recent years, various experimental methods such as tension [7–11], indentation [12–16], compression [17], shear [18], double cantilever beam [19] and bending tests [20–23] have been developed to measure the fracture strength and toughness of 8YSZ coatings as well as the interface adhesion strength of a TBC system. Due to the influence of bond coat, substrate and components with complicated structures, however, it is difficult to thoroughly study the mechanical properties of deposited 8YSZ top coatings. Only a few attempts have been made to directly measure the fracture features and mechanical parameters of freestanding 8YSZ coatings.

To further reveal the fracture behaviors of a TBC system, freestanding 8YSZ coating specimens were prepared by an air plasma sprayed (APS) technique, which were subjected to heat treatments for considering the sintering effect. Their mechanical properties, including the fracture strength σ_b and fracture toughness K_{IC} under thermal cycles, were measured by using single edge notched beam (SENB), an effective and credible method to test the fracture toughness of brittle ceramics [24]. The maximum bearing load of a notched specimen, defined as the failure or peak load, can be used for calculating σ_b and K_{IC}. In this paper, to clearly describe the crack initiation and propagation characteristics of APS 8YSZ, the bending fracture process near a pre-existed notch region was *in-situ* monitored by a non-contact and non-destructive digital image correlation (DIC) technique. The DIC data are advantageous in judging critical bending loads of notched freestanding 8YSZ samples and appraising other mechanical parameters. On the other hand, the variation of hardness H and K_{IC} of freestanding 8YSZ coatings were also measured by Vickers indentations [12]. The K_{IC} values were compared with that by the SENB tests. Finally, fracture morphologies of 8YSZ coatings were observed by scanning electron microscope and the effect of heat treatment on mechanical properties was discussed.

* Corresponding author at: Key Laboratory of Low Dimensional Materials & Application Technology, Ministry of Education, Xiangtan University, Hunan 411105, China. Tel.: +86 731 58298580; fax: +86 731 58292468.
E-mail addresses: ssamao@126.com, ssamao@xtu.edu.cn (W.G. Mao).

0921-5093/$ - see front matter © 2013 Elsevier B.V. All rights reserved.
http://dx.doi.org/10.1016/j.msea.2013.05.086

2. Experimental

2.1. Sample preparation

To prepare the stand-alone thick coating, the 8YSZ powder with grain sizes of 20–60 μm was directly sprayed on aluminum substrate with a size of $160 \times 25 \times 10\ mm^3$ by APS. During the APS process, substrate was cooled with the compressed air, resulting in deposition temperatures between 200 and 250 °C. After completing the spraying process and cooling to room temperature in air, the coated aluminum substrate was carefully incised into small bars by a commercial cutting machine (IsoMet® 4000). The top 8YSZ coating for each bar can be obtained after aluminum substrate was etched with potassium hydroxide. Then, these freestanding 8YSZ coatings were cut into rectangular-shape specimens with $20 \times 3 \times 4\ mm^3$. Each thermal cycling consists of 10 min heating to the desired surface temperature of 1000 °C, and then holding for 60 min, followed by a 10 min forced-air-quenching. All specimens were polished with 2.5 μm diamond paste. A total of 6 different annealing times of 0, 50, 100, 150, 200 and 300 were used. The number for each type of specimens is 5 and the total number of specimens is 60. Here, half of those were used for Vickers indentations and others were tested as SENB specimens. The specimens were fabricated and loaded according to the ASTM standard E1820-05a [24], where a notch was cut across the 3 mm face, perpendicular to the length of the bending bar. The narrow notch tip radii are about 5–10 μm by a commercial cutting machine with a thin diamond saw blade. The notch depths of ~1.5 mm were used, as shown in Fig. 1. The specimens were handled by hydrochloric acid to reduce the influence of surface work hardening. They were also carefully cleaned by an ultrasonic oscillator with distilled water and then completely dried.

2.2. SENB tests

There are two methods that were proposed to evaluate the critical bending load of a notched specimen in SENB tests. In the first method, the critical load is regarded as the peak point in a load-deflection curve, which is usually recorded by the universal testing machine. The second method is based on the DIC technique, which is used to monitor the strain evolution near the notch region, as illustrated by the dashed lines in Fig. 1. The strain burst deduced from the DIC data accurately reflects the crack nucleation and propagation of a notched specimen under bending, and then the corresponding load can be determined as the critical bending load [8]. Prior to the DIC testing, patterns were prepared by spraying a thin layer of black and white paint with airbrush guns. Based on the DIC technique, displacement fields were measured by tracking the features of random speckle patterns on the specimen surface [25]. A charge coupled device camera with 1624×1236 pixels and equipped by a lens of 50 mm focal length was used to *in-situ* measure the macroscopic morphology and strain evolution of the monitored region ($4 \times 3\ mm^2$) with a sampling rate of 2 images per second (see Fig. 1). The post-processing was achieved by the commercially available DIC software (ARAMIS) in order to analyze the evolution of a strain field. The measuring error of strain is less than 0.05% by calibration [26]. The compressive rate of the universal testing machine was set as 0.01 mm/min. The bending loads increase linearly up to the maximum, at which the notched 8YSZ samples break down. All experimental data, including the critical bending load, strain field, and crack initiation and propagation path, were *in-situ* recorded by a computer, which were used to estimate the mechanical properties of 8YSZ samples. In SENB tests, σ_b and K_{IC} can be obtained by [27]

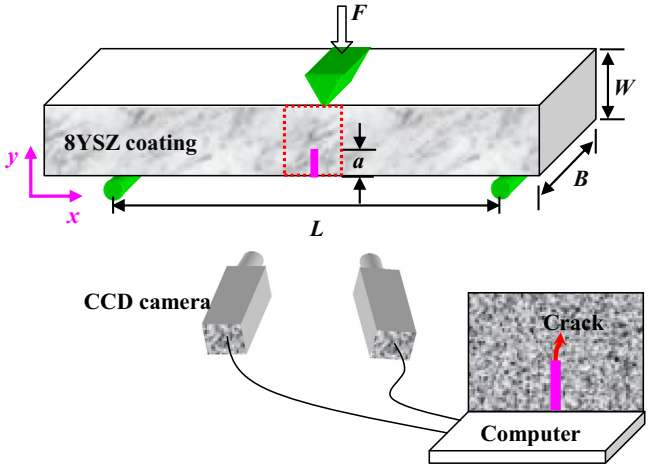

Fig. 1. Schematic of a typical SENB test by the aid of DIC. The rectangle with dashed lines is defined as a region for DIC monitoring.

$$\sigma_b = \frac{3FL}{2B(W-a)^2} \tag{1}$$

and

$$K_{IC} = Y\frac{3FL}{2BW^2}\sqrt{a}, \tag{2}$$

where F denotes the bending load, a is the initial length of a notch, B and W are, respectively, the width and height of the sample, L is the span between two lower supporting points, and Y is a factor defined as a/W. In the case of $L/W=4$, Y can be represented by the following exponential polynomial [28]:

$$Y = 1.93 - 3.07\frac{a}{W} + 14.53\left(\frac{a}{W}\right)^2 - 25.11\left(\frac{a}{W}\right)^3 + 25.8\left(\frac{a}{W}\right)^4 \tag{3}$$

2.3. Vickers indentation

The evolution of H and K_{IC} of undamaged freestanding 8YSZ specimens was measured by a modified Vickers indentation equipment [12]. Here it is worth noting that the effect of residual stress is ignored because it is small in freestanding 8YSZ specimens before and after heat treatments. In indentation tests, the loading time is 10 s, the dwelling time is 20 s at the peak load, and the unloading time is 15 s. Vickers micro-hardness impressions in TBCs are not as clearly defined as those in dense ceramics due to micro-cracks and porosity. To overcome this difficulty, the range of indentation loads was selected from 19.6 to 147 N in a modified Vickers indentation apparatus [12]. In Vickers indentation fracture tests, K_{IC} can be obtained as [29]

$$K_{IC} = \delta\left(\frac{E}{H}\right)^{1/2}\frac{P}{c^{3/2}} \tag{4}$$

where δ is a geometric factor and $\delta = 0.016$ for Vickers indenter, E and H are Young's modulus and micro-hardness of the sample, respectively, P is the indentation load, and c is the average length of two indentation cracks [12], as illustrated in Fig. 2. The indentation results were used to compare with that by the SENB measurements.

Owing to micro-cracks and pores in APS 8YSZ specimens, however, experimental results of H and K_{IC} exhibit a large scatter. It is known that the Weibull distribution can be applied to describe the scatter of mechanical properties of brittle materials [30–32]. Based on the Weibull statistics, the cumulative distribution p of a measured parameter x can be represented as [31]

$$p = 1 - \exp\left[-\left(\frac{x}{x_0}\right)^m\right] \tag{5}$$

where x_0 and m are the normalized tested parameter and Weibull modulus, respectively. Here, experimental data are sorted in an

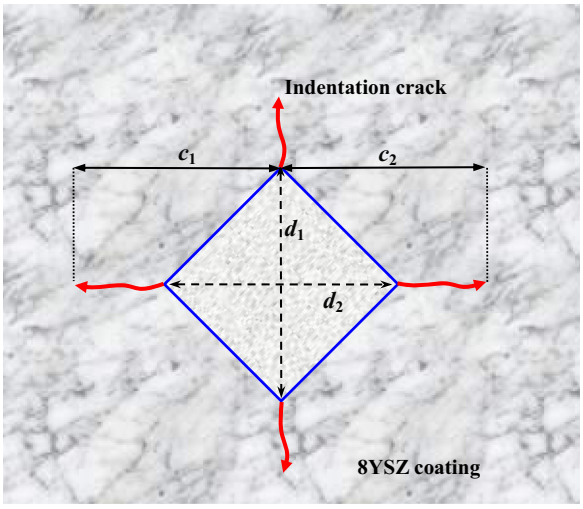

Fig. 2. Schematic of the fracture toughness measurement of brittle ceramic coatings by Vickers indentation.

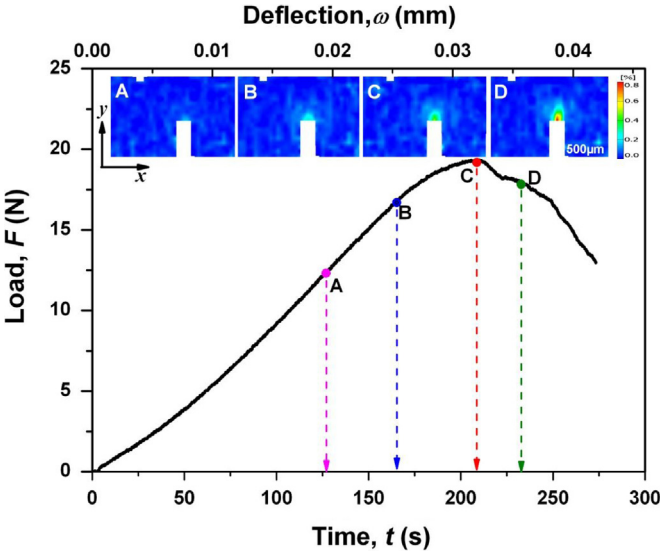

Fig. 3. A typical loading-deflection-time curve of 8YSZ samples during SENB. A series of strain mapping (insets A, B. C and D) show the evolution of strain in the monitored area with the increase of bending loads at $N=200$.

ascending order and each value is assigned to a probability of $p=(i-0.5)/n$, where i is the i-th rank and n is the total number of tests [32].

3. Results and discussion

3.1. Fracture features

As shown in Fig. 3, the correlation between bending loads and DIC mapping can be described as a function of time, which is utilized to accurately judge the crack propagation and coating failure. The deflection ω and longitudinal strain ε_{xx} in the dashed region (see Fig. 1) slowly increase with the increase of F. To estimate the critical stain transition point and then determine the critical bending load, the ε_{xx} data for each 8YSZ sample were linearly fitted in slow and rapid growth stages, respectively (see inset in Fig. 4). The two fitted lines intersect at point M. Another line can be plotted along the half of their angle, which intersects with the experimental curve at point N. Therefore, the corresponding time can be approximately regarded as

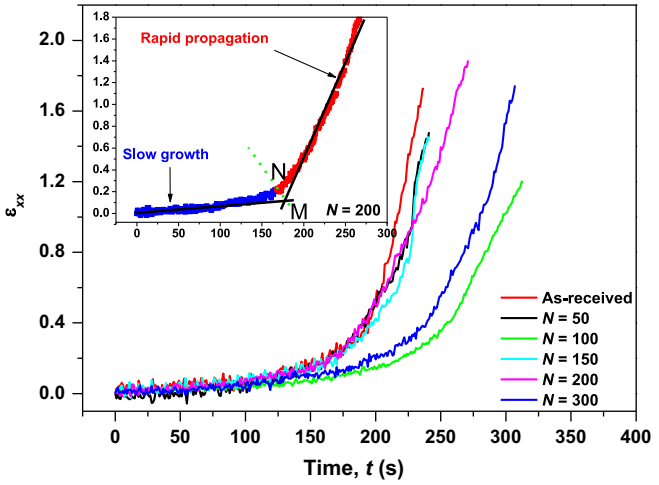

Fig. 4. Relationship of ε_{xx} by DIC in the monitored region *versus* loading time during bending tests.

Table 1
Comparison of fracture strengths of freestanding 8YSZ coatings obtained by SENB and DIC tests.

N	E (GPa)	ε_{xx}^{cri}	σ_b* (MPa)	σ_b** (MPa)	σ_b*** (MPa)
0	9.78 ± 1.00	0.28 ± 0.02	27.38 ± 1.96	35.66 ± 6.13	37.72 ± 5.21
50	22.41 ± 1.20	0.23 ± 0.03	51.54 ± 6.72	71.76 ± 7.25	77.50 ± 6.52
100	29.68 ± 2.23	0.19 ± 0.02	56.39 ± 5.94	53.90 ± 1.87	61.20 ± 1.88
150	31.01 ± 1.34	0.18 ± 0.02	56.90 ± 6.32	56.05 ± 0.72	60.59 ± 1.15
200	34.66 ± 1.57	0.15 ± 0.02	51.99 ± 6.93	31.62 ± 1.21	36.35 ± 1.14
300	32.41 ± 2.68	0.17 ± 0.04	55.10 ± 12.9	24.70 ± 0.40	25.65 ± 0.42

* σ_b was directly calculated by ε_{xx}^{cri} and E based on linear elastic facture mechanics.
** σ_b was estimated by SENB with Eq. (1) and F_{cr}^{DIC}.
*** σ_b was obtained by SENB with Eq. (1) and F_{cr}.

the critical fracture time. Then, the critical bending load F_{cr}^{DIC} and longitudinal strain ε_{xx}^{cri} were determined, respectively, by the recorded data with the universal test machine and DIC apparatus. For example, as shown by inset A in Fig. 3, the strain variation measured by DIC near the notch tip reveals no apparent change before $t=126$ s. As F increases, ω grows linearly. At $t=167$ s, a strain concentration deduced from the DIC data appears near the notch tip (see inset B in Fig. 3), where $F=17.01$ N. This indicates that a crack has been formed near the notch tip. Here, the critical strain, ε_{xx}^{cri}, equals $0.21\pm0.02\%$ and $t=167$ s. As F further increases, ω and the strain concentration become more visible. At $t=208$ s, the specimen loses the whole bearing capacity and ruptures along the pre-existed notch direction at $F=19.35$ N (see inset C in Fig. 3). The load rapidly decreases to 17.93 N after $t=232$ s (see inset D in Fig. 3). In the traditional SENB method, the peak load $F=19.35$ N at point C is usually regarded as the critical load F_{cr} in Eqs. (2) and (4). However, the DIC data clearly show that a crack has initiated when $F=17.01$ N at point B, *i.e.*, before F arrives to F_{cr}. In this paper, the bending load evaluated by DIC is regarded as the critical load F_{cr}^{DIC}, which is slightly less than F_{cr} determined by the conventional SENB. This may improve the testing accuracy in evaluating the mechanical properties of brittle ceramic coatings.

3.2. Determination of σ_b and K_{IC} by SENB and DIC

As listed in Table 1, the σ_b evolution of each notched 8YSZ sample before and after heat treatments was evaluated by the SENB and DIC methods. In SENB tests, σ_b obtained by F_{cr} or F_{cr}^{DIC} represents a similar trend with the increasing of thermal aging time. It firstly increases with thermal cycles due to the sintering effect, and then slowly

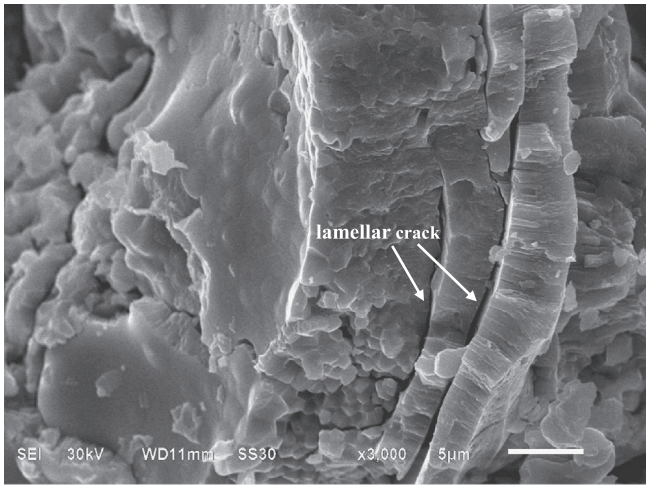

Fig. 5. Typical scanning electron microscope graph of fracture surface of free-standing 8YSZ samples after SENB tests, where $N=200$.

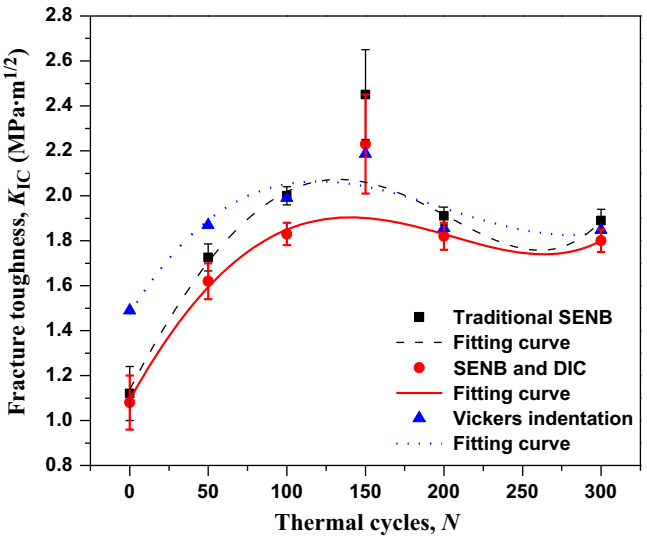

Fig. 6. Variation of fracture toughness of freestanding 8YSZ coatings with thermal cycles.

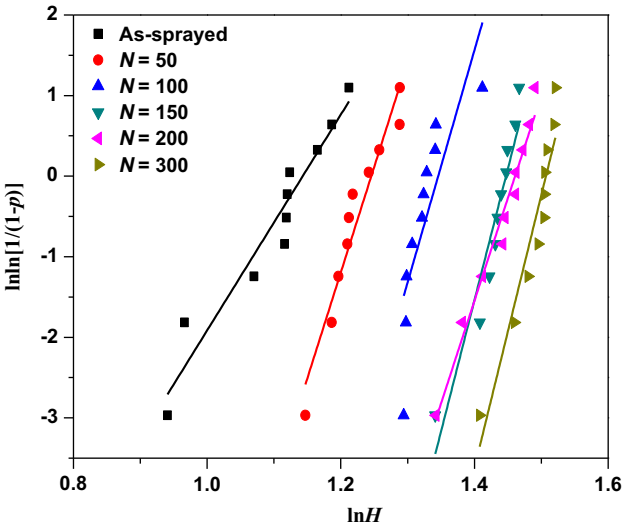

Fig. 7. Weibull plot of hardness of 8YSZ coatings by Vickers indentations.

decreases to the initial value because of micro-crack nucleation and delamination. To further explain this phenomenon, the fracture morphology after SENB was observed by scanning electron microscope, as shown in Fig. 5. It is seen that there are a large amount of pores in conjunction with splat structures for annealed APS coatings. It mainly exhibits the inter-splats fracture mode. After 200 thermal cycles, a noticeable sintering phenomenon occurs owing to the phase transformation and substantial grain growth of 8YSZ ceramics [33,34]. It may result in the increase of mechanical properties (E, σ_b and K_{IC}) of 8YSZ coatings. The similar phenomena have been reported in previous experiments [35–37]. With the increase of thermal cycling, more and more lamellar micro-cracks would degrade the strength of 8YSZ coatings. In addition, it is seen that the results deduced by F_{cr} in Table 1 are 5.78%, 8.00%, 13.54%, 8.10%, 14.96% and 3.85% larger than that determined by F_{cr}^{DIC}, respectively, at $N=0$, 50, 100, 150, 200, and 300. The reason may be attributed to the difference of critical bending loads. On the other hand, using the results of ε_{xx}^{cri} obtained by DIC and E from our early work [38], σ_b of freestanding 8YSZ coatings can be directly calculated by $\varepsilon_{xx}^{cri}\cdot E$ based on linear elastic fracture mechanics, as listed in Table 1. It is seen that σ_b increases from the as-received value of 27.38 ± 1.96–56.90 ± 6.32 MPa at $N=150$ with increasing the thermal aging time, and then reaches a plateau of 55.10 ± 12.8 MPa at $N=300$, which agrees well with the results obtained by four-point bending tests [3]. The quantitative agreement between the results by $\varepsilon_{xx}^{cri}E$ and that by using Eq. (1) and F_{cr}^{DIC} shows that, in SENB tests, F_{cr}^{DIC} determined by DIC is more suitable to analyze the fracture characteristics of brittle ceramics than F_{cr} by traditional SENB tests.

Similarly, using Eq. (2) and the critical bending load F_{cr}, K_{IC} of heat-treated 8YSZ specimens changes from 1.12 to 2.45 MPa m$^{1/2}$ before $N=150$ and decreases to 1.89 MPa m$^{1/2}$ at $N=300$, as shown in Fig. 6. The relevant K_{IC} estimated by F_{cr}^{DIC} that corresponds to the appearance of strain concentration and crack nucleation changes from 1.04 to 2.23 MPa m$^{1/2}$ prior to $N=150$ thermal cycles, and decreases to 1.8 MPa m$^{1/2}$ at $N=300$. These results are slightly less than that by SENB. According to earlier experiments, K_{IC} for an APS TBCs system is 1.15 ± 0.07 MPa m$^{1/2}$ by asymmetric four-point bending tests at room temperature [39], and 0.7–1.2 MPa m$^{1/2}$ by Vickers indentation tests [12]. Thus, it is obvious that the results are in agreement with available data.

3.3. Evaluation of K_{IC} by Vickers indentation

As shown in Fig. 7, the scattered data of H can be well fitted by the Weibull distribution for as-received and heat-treated 8YSZ specimens, where the normalized hardness is, respectively, equal to 3.12, 3.48, 3.84, 4.25, 4.31 and 4.51 GPa. It increases with the increase of thermal cycles, which is attributed to the effect of high-temperature sintering. Choi et al. [38] showed that H for APS 8 YSZ coatings increases from the as-received value of 2.34–4.49 GPa when the thermal aging time equals about 5 h. Then, it gradually approaches a plateau of 4.36 GPa after annealing 500 h [3]. The results in this paper are in agreement with these data, but they are less than that of nano-structured APS YSZ coatings [40]. Similarly, using the given H, E and Eq. (4), K_{IC} of each type of freestanding 8YSZ samples can be obtained by the Weibull statistical analysis, as shown in Fig. 8. The normalized K_{IC} is equal to 1.53, 1.95, 2.06, 2.25, 1.97 and 1.81 MPa m$^{1/2}$, as shown in Fig. 6. Compared with the SENB data, the results by Vickers indentations are slightly more than that by SENB before $N=150$. Then, they gradually decrease and tend to consist with that by SENB and DIC tests.

4. Conclusions

The fracture characteristics and evolution of mechanical properties of freestanding 8YSZ coatings play an important role in

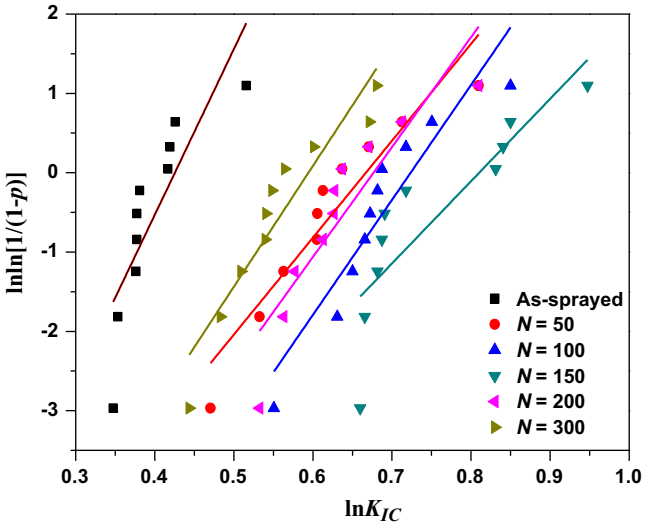

Fig. 8. Weibull plot of fracture toughness of 8YSZ coatings by Vickers indentations.

appraising the reliability and durability of a TBC system. In this paper, the mechanical properties of freestanding 8YSZ samples were measured by SENB with the help of DIC and Vickers indentations, respectively. The main conclusions can be summarized as follows:

(1) The strain fields and crack nucleation near the pre-existed notch were successfully *in-situ* monitored by DIC during SENB tests, which are instructive to judge the critical bending load and improve the measurement accuracy.
(2) The fracture strength of freestanding 8YSZ coatings was evaluated by three different methods. It approximately increases from 30 to 55 MPa with the increase of thermal cycles due to the effect of sintering and phase transformation.
(3) The fracture toughness of freestanding 8YSZ coatings measured by SENB and DIC is slightly less than that by the conventional SENB method. It changes from 1.04 to 2.23 MPa $m^{1/2}$ before $N=150$, and then decreases to 1.8 MPa $m^{1/2}$ at $N=300$. K_{IC} by Vickers indentation is equal to 1.53, 1.95, 2.06, 2.25, 1.97 and 1.81 MPa $m^{1/2}$ for various thermal aged 8YSZ samples. The results qualitatively consist with that by SENB and DIC tests.

Acknowledgments

This work has been supported by the Key Project of Scientific Research Innovation of Hunan Provincial Department of Science and Technology (No. 2011TT1006), the Project of Teaching Innovation of Hunan Provincial Ordinary High School (No. 2012401), the National Natural Science Foundation of China (Nos. 11102177, 11227801 and 11272276), the Natural Science Foundation of Hunan Province for Innovation Group (No. 09JJ7004), and the Program for Changjiang Scholars and Innovative Research Team (No. IRT1080).

References

[1] A.G. Evans, M.Y. He, J.W. Hutchinson, Prog. Mater. Sci. 46 (2001) 249–271.
[2] A.F. Renteria, B. Saruhan, J. Eur. Ceram. Soc. 26 (2006) 2249–2255.
[3] S.R. Choi, D. Zhu, R.A. Miller, J. Am. Ceram. Soc. 88 (2005) 2859–2867.
[4] D. Casellas, A. Feder, L. Llanes, M. Anglada, Scripta Mater. 45 (2001) 213–220.
[5] J. Wu, H. Guo, M. Abbas, S. Gong, Prog. Nat. Sci. Mater. Int. 22 (2012) 40–47.
[6] W.O. Soboyejo, P. Mensah, R. Diwan, J. Crowe, S. Akwaboa, Mater. Sci. Eng. A 528 (2011) 2223–2230.
[7] W.B. Yao, C.Y. Dai, W.G. Mao, C. Lu, L. Yang, Y.C. Zhou, Surf. Coat. Technol. 206 (2012) 3803–3807.
[8] D.J. Wu, W.G. Mao, Y.C. Zhou, C. Lu, Appl. Surf. Sci. 257 (2011) 6040–6043.
[9] W. Shen, F. Wang, Q. Fan, Z. Ma, X. Yang, Surf. Coat. Technol. 205 (2011) 2964–2969.
[10] C.S. Ramachandran, V. Balasubramanian, P.V. Ananthapadmanabhan, Surf. Eng. 27 (2011) 217–229.
[11] Z.B. Chen, Z.G. Wang, S.J. Zhu, Surf. Coat. Technol. 205 (2011) 3931–3938.
[12] W.G. Mao, J. Wan, C.Y. Dai, J. Ding, Y. Zhang, Y.C. Zhou, C. Lu, Surf. Coat. Technol. 206 (2012) 4455–4461.
[13] T. Zisis, N.A. Fleck, Wear 268 (2010) 443–454.
[14] Y. Yamazaki, S. Kuga, T. Yoshida, Acta Metall. Sin. (Engl. Lett.) 24 (2011) 109–117.
[15] A. Dey, A.K. Mukhopadhyay, J. Int., Appl. Ceram. Technol. 8 (2011) 572–590.
[16] X. Wang, C. Wang, A. Atkinson, Acta Mater. 60 (2012) 6152–6163.
[17] W.G. Mao, C.Y. Dai, Y.C. Zhou, Q.X. Liu, Surf. Coat. Technol. 201 (2007) 6217–6227.
[18] Z. Xu, Y. Yang, P. Huang, X. Li, Acta Mater. 58 (2010) 5972–5979.
[19] E.M. Donohue, N.R. Philips, M.R. Begley, C.G. Levi, Mater. Sci. Eng. A 564 (2013) 324–330.
[20] C. Pfeiffer, E. Affeldt, M. Göken, Surf. Coat. Technol. 205 (2011) 3245–3250.
[21] P.F. Zhao, C.A. Sun, X.Y. Zhu, F.L. Shang, C.J. Li, Surf. Coat. Technol. 204 (2010) 4066–4074.
[22] X. Wang, S. Tint, M. Chiu, A. Atkinson, Acta Mater. 60 (2012) 3247–3258.
[23] J. Malzbender, R.W. Steinbrech, Surf. Coat. Technol. 209 (2012) 97–102.
[24] Standard Test Method for Measurement of Fracture Toughness E1820-05a. ASTM International, West Conshohocken, 2005.
[25] C. Efstathiou, H. Sehitoglu, J. Carroll, J. Lambros, H.J. Maier, Acta Mater. 56 (2008) 3791–3799.
[26] W.G. Mao, D.J. Wu, W.B. Yao, M. Zhou, C. Lu, J. Appl. Phys. 110 (2011) 084903.
[27] J.B. Wachtman, Mechanical Properties of Ceramics, John Wiley & Sons Inc., New York, 1996.
[28] W.F. Brown, J.E. Srawley, Plane Strain Crack Toughness Testing of High Strength Metallic Materials, American Society for Testing and Materials, Philadelphia, 1966.
[29] D.B. Marshall, B.R. Lawn, J. Am. Ceram. Soc. 60 (1977) 86–87.
[30] T.Y. Zhang, L.Q. Chen, R. Fu, Acta Mater. 47 (1999) 3869–3878.
[31] W. Weibull, S. Sweden, J. Appl. Mech. 18 (1951) 293–297.
[32] C. Lu, R. Danzer, F.D. Fischer, Phys. Rev. E 65 (2002) 067102.
[33] J. Wu, H.B. Guo, L. Zhou, L. Wang, S.K. Gong, J. Therm. Spray Technol. 19 (2010) 1186–1194.
[34] K. Wang, H. Peng, H. Guo, S. Gong, Chin. J. Aeronaut. 25 (2012) 811–816.
[35] S. Guo, Y. Kagawa, Scr. Mater. 50 (2004) 1401–1406.
[36] J.A. Thompson, T.W. Clyne, Acta Mater. 49 (2001) 1565–1575.
[37] F. Tang, J.M. Schoenung, Scr. Mater. 54 (2006) 1587–1592.
[38] W.G. Mao, Q. Chen, C.Y. Dai, L. Yang, Y.C. Zhou, C. Lu, Surf. Coat. Technol. 204 (2010) 3573–3577.
[39] S.R. Choi, D. Zhu, R.A. Miller, Eng. Fract. Mech. 72 (2005) 2144–2158.
[40] B. Liang, G. Zhang, H.L. Liao, C. Coddet, C.X. Ding, J. Therm. Spray Technol. 19 (2010) 1163–1170.